Available online at www.sciencedirect.com
SCIENCE DIRECT®

Cryobiology 53 (2006) 75–95

CRYOBIOLOGY

www.elsevier.com/locate/ycryo

Fracture formation in vitrified thin films of cryoprotectants ☆

Yoed Rabin *, Paul S. Steif, Katherine C. Hess, Jorge L. Jimenez-Rios, Matthew C. Palastro

Biothermal Technology Laboratory, Department of Mechanical Engineering, Carnegie Mellon University, 5000 Forbes Avenue, Pittsburgh, PA 15237, USA

Received 15 December 2005; accepted 9 March 2006
Available online 19 June 2006

Abstract

As a part of an ongoing effort to study the continuum mechanics effects associated with cryopreservation, the current report focuses on fracture formation in vitrified thin films of cryoprotective agents. The current study combines experimental observations with continuum mechanics analysis. Experimental results have been developed using a new imaging device, termed a "cryomacroscope", which has been recently presented by the current research team. A newly developed liquid nitrogen-based cooling stage is presented in this paper. The samples under investigation are 0.5 ml droplets of cryoprotective agents, having a characteristic diameter of 20 mm and a characteristic thickness of 1.5 mm. Tested samples included dimethyl sulfoxide (DMSO) in a concentration range from 6 to 8.4 M, and the cryoprotectant cocktails VS55 and DP6. Some samples contained small bovine muscle segments, having a characteristic dimension of 1 mm, in order to study stress concentration effects. Experimental results show that the onset of fracturing in vitrified films of cryoprotectants is very consistent, occurring over a small temperature range. Fracture pattern, however, was affected by the cooling rate. The presence of tissue segments did not affect the onset temperature of fracture, but affected the fracture pattern. The continuum mechanics analysis solidified the hypothesis that fracture is driven by thermal stress, not by temperature per se, and allowed fracture strain to be inferred from observed fracture temperature. In conjunction with the current report, additional photos of fracture formation in thin films are available at http://www.me.cmu.edu/faculty1/rabin/CryomacroscopyImages02.html.

Keywords: Cryomacroscopy; Vitrification; Continuum mechanics; Fracture; DMSO; VS55; DP6; Set-temperature

One of the many factors that impact the survival and integrity of living biological tissues during cryopreservation is the development of mechanical stress [6,7,11,34] (also termed "thermal stress"). Thermal stress is driven by the phenomenon of thermal expansion [16–18,21–23,27], with fracture formation as its most dramatic outcome [6,11,24,26,31]. The study of thermal stress effects in cryobiology can be classified with respect to the process of freezing: by crystallization, by vitrification (i.e., glass formation; vitreous in Latin means glass), or by a combination of both.

Of those freezing processes, mathematical modeling of thermal stress during crystallization (such as the case in cryosurgery) is the least complex

☆ This study has been supported in part by NHLBI, Grant No. R01 HL069944.
* Corresponding author. Fax: +1 412 268 3348.
E-mail address: Rabin@CMU.EDU (Y. Rabin).

0011-2240/$ - see front matter © 2006 Elsevier Inc. All rights reserved.
doi:10.1016/j.cryobiol.2006.03.013

[5,19,20]. Here, the material is most conveniently subdivided into regions according to the phase of state, where the frozen material is typically assumed to behave like a linear-elastic material, having a linear relationship between strain and stress (or between elongation and load in the special case of uni-axial loading). The unfrozen material is assumed to behave like a stationary liquid, incapable of supporting any shear stress. Additional model assumptions must be made when phase transition occurs over a temperature range, which is typically the case in biological materials. However, experimental evidence on the mechanical behavior of the material in the phase transition temperature range is largely unknown.

While the mathematical modeling of thermal stress during vitrification is largely uncharted, concepts from the general field of continuum mechanics clearly must be drawn upon. Analysis must account for the elevation of the viscosity by fourteen orders of magnitude associated with cooling the material from room temperature to the so-called glass transition temperature [15,27]; this dramatic property change produces a continuous transformation from a liquid-like material to a solid-like material. Stresses in a vitrified material would produce both elastic (instantaneous) deformation, as well as "creep" or viscous deformation. In creep, the strain increases continually under constant stress, where the creep strain rate is inversely proportional to the viscosity. Creep is related to stress relaxation, which refers to the decrease (relaxation) of stress over time when a material is subjected to a sudden increase in strain. Creep strain dominates elastic strains at higher temperatures; with a decrease in temperature, the elastic strain becomes comparable to, and eventually dominates, creep strain.

While complete vitrification can potentially prevent the devastating effect of ice crystallization [30], the high concentration of the cryoprotective agents involved in it is potentially very toxic [7,10,12,32,33]. Cryopreservation subject to a low concentration cryoprotective agent (CPA) and sub-critical cooling rates to promote vitrification, is widely known as classical cryopreservation. In classical cryopreservation, ice crystals first nucleate at about the heterogeneous nucleation point for the specific cryoprotectant composition, while the concentration of the remaining solution elevates. The progress of crystal formation, and elevation of the concentration of the remaining solution, continues with cooling, until the remaining solution becomes so viscous as to form glass at the particular cooling rate [16]. One could view classical preservation as localized vitrification in small regions, or "pockets". The volume fraction eventually occupied by ice crystals is affected by many factors, and the coexistence of crystallized and vitrified regions is an inevitable outcome of classical cryopreservation.

Modeling of classical cryopreservation is a very challenging task; the formation of pockets of vitrified material are statistical events that are difficult to predict. It seems that continuum mechanics effects associated with classical cryopreservation can be modeled only after cryopreservation by vitrification alone is better understood in the continuum mechanics sense. Many continuum mechanics effects in the vitrification of biomaterials are presently unexplored.

The current study is designed to explore one aspect of the continuum mechanics of cryopreservation for vitrifying materials: fracture formation in thin films. More specifically, the current study seeks to investigate the repeatability and consistency of fracture formation in vitrified cryoprotectants, in the presence and absence of tissue segments. This study is focused on DMSO in the concentration range of 6 to 8.4 M, and the cryoprotectant cocktails VS55 and DP6. Thermal stress analysis is combined with experimental results to interpret events associated with thermal stress during vitrification.

Materials and methods

Fig. 1 presents a schematic illustration of the experimental apparatus. The cryomacroscope setup has been presented recently [26] and is described here in brief only, followed by a detailed description of a cooling mechanism, which was developed especially for the purpose of the current study. The experimental apparatus was designed and constructed at the Biothermal Technology Laboratory of the Department of Mechanical Engineering, at Carnegie Mellon University.

With reference to Fig. 1, the cryomacroscope comprises a 12 in. rigid borescope (Gradient Lens Corporation, Inc., model Hawkeye Slim HH12-AF, 42° view angle), a light source (Gradient Lens Corporation, Inc., Mini-Maglite®), a video coupler lens (Gradient Lens Corporation, Inc., model Luxxor 35 mm FL), a Hyper HAD CCD camera (Costar, Inc., model SI-M350, 768×494 pixels), a time/date stamp generator (Crest Electronics, Inc., model TDG/2001), a video grabber (Hewlett-Pack-

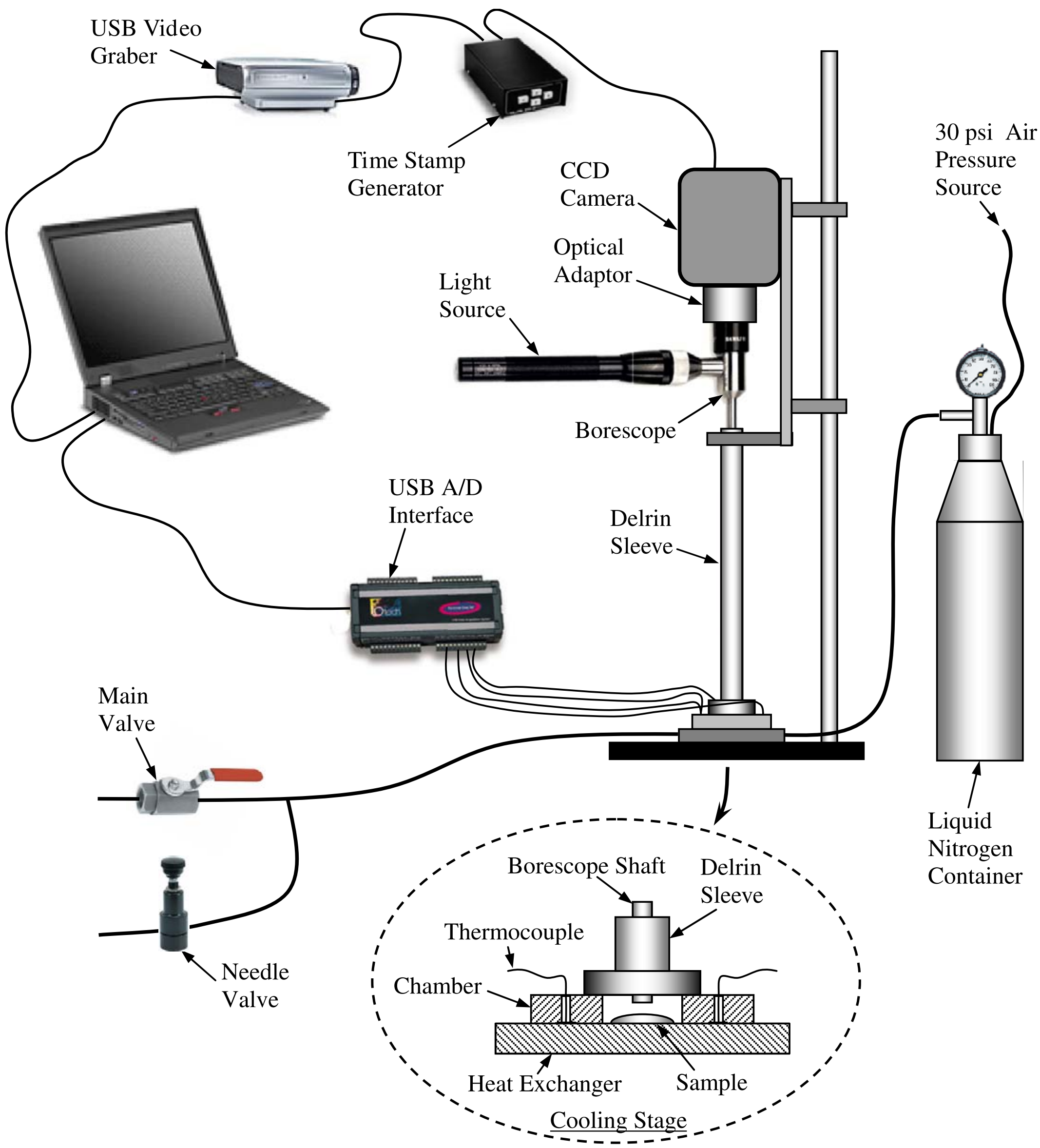

Fig. 1. Schematic illustration of the cryomacroscope setup.

ard, Inc., model dc5000), a personal computer, and a USB data acquisition module for thermocouple temperature measurements (OMB-DAQ-55, Omega Engineering, Inc.). The borescope, light source, optical coupler, and the CCD camera are mounted on a frame, with the additional support of a delrin sleeve. That assembly can be moved in the vertical direction, to adjust the magnification of imaging. The combination of the camera resolution of 768×494 pixels, a depth of field of 28 mm (the height of the cooling chamber in Fig. 2), and a view angle of 42°, makes each pixel of the CCD camera equivalent to a 28 μm diameter circle on the cooling stage surface. This defines the smallest fracture observable by the specific cryomacroscope setup, which is a few orders of magnitude smaller than the typical length of fracture in the current samples.

The cooling mechanism comprises an air pressure source of 30 psi, a vacuum insulated liquid nitrogen container, a cooling stage, and two nitrogen flow valves. The combination of the air pressure source and the liquid nitrogen container provides a constant heat sink on demand. To create various thermal histories for experimentation, the actual

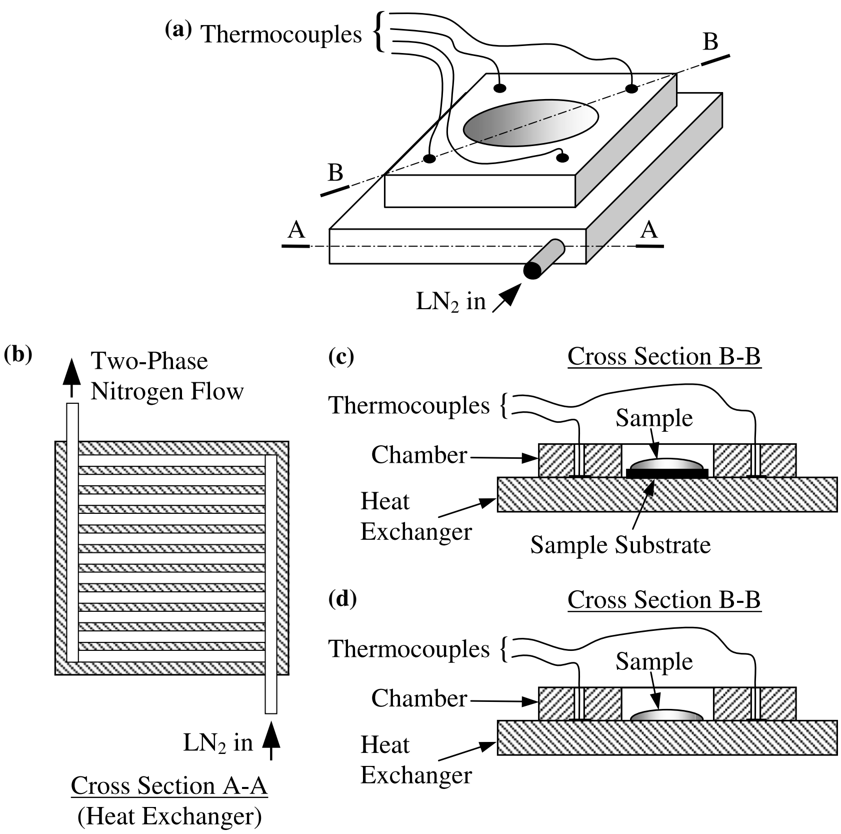

Fig. 2. Schematic illustration of the cooling stage: (a) a general view, (b) a horizontal cross section through the heat exchange, and a vertical cross section through the cooling stage with (c), and without (d), a substrate (a thin sheet of glass or plastic).

nitrogen flow rate through the cooling stage is controlled by the two-valve configuration. Below the heterogeneous nucleation point of the sample, vitrification requires a cooling rate higher than some threshold rate, depending on the material properties. The threshold cooling rate is inversely proportional to the sample's viscosity, and since the viscosity value increases exponentially with decrease in temperature, the same threshold cooling rate decreases exponentially with the decrease in temperature. The two-valve setup illustrated in Fig. 2 is designed to create two different ranges of cooling rates during the experiment. The main valve is completely opened at the initiation of cooling, leading to a maximum cooling rate of the cooling stage. Once the main valve is turned off, a preset opening of the needle valve dominates the nitrogen flow rate and, thereby, the cooling rate. In the current study, the main valve was turned off when the sample temperature reached −120 °C. The relationship between the needle position of the valve and cooling rate was studied in a sequence of training sessions, prior to obtaining the experimental results reported in this study. The relationship between the cooling rate and the onset of fracturing is one of the effects analyzed in this study.

The sample

The sample in this study is a 0.5 ml cryoprotectant droplet resting on a flat surface, which naturally formed a circular thin film with a typical thickness of 1.5 mm and a typical diameter of 20 mm (thin in the continuum mechanics sense where the diameter is more than 10 times the thickness). The current study includes experimental observations on DMSO in a concentration range of 6–8.4 M, as well as the cryoprotectant cocktails DP6 and VS55. DP6 is a cocktail of 234.4 g/l DMSO (3 M), 228.3 g/l propylene glycol (3 M), and 2.4 g/l HEPES in a EuroCollins solution. VS55 is a cocktail of 242.14 g/l DMSO (3.1 M), 168.38 g/l propylene glycol (2.2 M), 139.56 g/l formamide (3.1 M), and 2.4 g/l Hepes in a EuroCollins solution. The two cocktails are similar, except for the exclusion of formamide from DP6. In return, the DP6 contains a higher concentration of propylene glycol [17,23]. For comparison purposes, the specific DMSO concentration of 7.05 M was studied, which contains the same overall mass of solutes as in the cocktail of VS55 [17]. The VS55 and DP6 cocktails were prepared at Cell and Tissue Systems, Inc. (Charleston, SC).

In order to gain insight into the effect of tissue samples on fracture formation, a few bovine muscle segments were further immersed in selected cryoprotectant samples. Those tissue segments had typical lineal dimension of 1 mm, and they were permeated with the cryoprotectant for at least 24 h prior to experimentation. At the end of the permeation period, and as a part of sample preparations, the tissue segments were immersed in a new droplet of cryoprotectant, to eliminate dilution of the cryoprotectant droplet.

The cooling stage

With reference to Fig. 2, the cooling stage comprises a multi channel heat exchanger made of copper. Typical dimensions of the heat exchanger are 60 mm × 60 mm × 9.5 mm, and the channel diameter is 3 mm. The cooling chamber is created by a 28 mm thick plexiglass plate, having a cylindrical hole of 35 mm in diameter at its center, enclosed between the upper surface of the heat exchanger and the lower base of the delrin sleeve (bottom of Fig. 1).

Since direct temperature measurements by immersing a temperature sensor into the sample may affect fracture formation, and due to the fact that copper has an extremely high thermal conductivity (which further increases with the decrease in temperature), a four thermocouple array, surrounding the sample from all sides, was used to measure the cooling stage temperature. Four holes were drilled in the plexiglass plate for that purpose, at the four corners of an imaginary square, 35 × 35 mm in size. The average temperature of the four thermocouples is estimated to be the sample temperature. Due to the extremely high value of thermal resistance to heat transfer by convection from the sample to the air, when compared with the resistance to heat transfer by conduction across the film, the temperature variation across the film is negligible.

The driving mechanism for fracture formation in the sample is the thermal expansion difference between the cryoprotectant and the heat exchanger, and the constraint imposed by the heat exchanger on the cryoprotectant. In order to obtain additional evidence as to the driving mechanism for cracking, a series of additional experiments were carried out in which sample substrates of various materials were used (Fig. 2c): 1 mm glass plate (microscope cover slide), 150 μm glass plate (microscope cover slide), 120 μm plastic film (transparency of an overhead projector), and 30 μm plastic film (plastic wrap for food storage). The analysis of this effect is discussed in the continuum mechanics analysis section below. To obtain reliable temperature measurements when a substrate of a different material was placed between the copper heat exchanger and the cryoprotectant sample, four additional identical substrates were placed between the contact point of each thermocouple and the copper heat exchanger, with the goal of creating similar thermal conditions for the thermocouples and the sample.

Experimental results and discussion

Table 1 presents a summary of experimental results from 97 experiments on various concentrations of DMSO, 52 experiments on VS55, and 41 experiments on DP6. The number of fractured samples, n_f, out of the total number of tested samples, n_t, is also listed in Table 1 for each set of experimental conditions. However, n_f is only an indication of whether fracture formation took place, not the intensity of fracturing. Not only did fractures occur in only one half of the samples placed on the 30 μm plastic substrate, but the intensity of fractures in those experiments was also dramatically lower, when compared with, for example, experiments on a 120 μm plastic substrate. It is acknowledged that the term "fracture intensity" is used here as a qualitative measure only, where quantification of this effect is yet not established.

The fracture temperature, T_f, listed in Table 1 is the average temperature of the four thermocouples located at the four corners of the cooling stage. The reason for the temperature variation is the pattern of flow in the heat exchanger, where the highest temperature is near the inlet, and the lowest temperature is near the outlet. The maximum temperature difference is a function of the boiling regime in the channels, as well as of the mass flow rate of the liquid nitrogen. The maximum temperature difference between these thermocouples is listed as ΔT_{fm}. Since the typical diameter of the sample is 20 mm

Table 1
Summary of experimental work, where n_f is the number of fractured specimens, n_t is the total number of experiments, T_f is the fracture temperature, ΔT_{fm} is the maximum temperature difference along the cooling stage at the onset of fracturing, and ΔT_{fs} is the estimated temperature difference along the sample at the onset of fracturing (uncertainty in the table is represented as one standard deviation)

Cryoprotectant	Substrate	Muscle segments	n_f/n_t	T_f, °C	ΔT_{fm}, °C	ΔT_{fs}, °C
6.5 M DMSO	None	−	8/8	−143.7 ± 1.9	2.6 ± 1.3	1.5 ± 0.7
	None	+	6/6	−142.3 ± 1.2	3.0 ± 1.4	1.7 ± 0.8
7.05 M DMSO	None	−	11/11	−141.7 ± 1.9	3.2 ± 1.2	1.8 ± 0.7
	None	+	5/5	−142.2 ± 1.2	3.5 ± 2.0	2.0 ± 1.1
	1 mm Glass	−	6/6	−145.2 ± 2.2	11.7 ± 3.4	6.7 ± 1.9
	150 μm Glass	−	9/9	−159.1 ± 5.4	5.4 ± 2.5	3.1 ± 1.4
	120 μm Plastic	−	4/10	−164.3 ± 3.0	5.2 ± 3.1	3.0 ± 1.8
	30 μm Plastic	−	3/7	−144.0 ± 3.2	6.3 ± 3.0	3.6 ± 1.7
8 M DMSO	None	−	10/11	−141.1 ± 1.7	2.9 ± 1.5	1.7 ± 0.9
	None	+	6/6	−138.0 ± 0.8	2.4 ± 1.3	1.4 ± 0.7
8.4 M DMSO	None	−	12/12	−142.8 ± 3.5	2.7 ± 1.4	1.5 ± 0.8
	None	+	6/6	−138.5 ± 1.8	2.6 ± 1.5	1.5 ± 0.9
VS55	None	−	17/18	−134.7 ± 2.1	2.5 ± 1.1	1.4 ± 0.6
	None	+	10/10	−135.5 ± 2.7	5.0 ± 1.8	2.9 ± 1.0
	1 mm Glass	−	4/6	−144.8 ± 13.0	6.0 ± 1.3	3.4 ± 0.7
	150 μm Glass	−	8/10	−158.6 ± 9.6	8.1 ± 3.6	4.6 ± 2.1
	120 μm Plastic	−	0/3	—	—	—
	30 μm Plastic	−	4/5	−134.0 ± 1.0	5.2 ± 0.4	3.0 ± 0.2
DP6	None	−	6/6	−133.2 ± 3.2	5.5 ± 1.0	3.1 ± 0.6
	None	+	0*/6	—	—	—
	1 mm Glass	−	6/7	−137.5 ± 6.9	18.5 ± 10.3	10.6 ± 5.9
	150 μm Glass	−	7/7	−160.7 ± 6.6	7.7 ± 3.7	4.4 ± 2.1
	120 μm Plastic	−	3/7	−154.5 ± 10.1	8.7 ± 2.2	5.0 ± 1.3
	30 μm Plastic	−	3/8	−155.8 ± 0.7	5.7 ± 1.3	3.3 ± 0.7

* All samples crystallized.

and the typical distance between the thermocouples is 35 mm, ΔT_{fs} represents an estimated upper limit for temperature difference along the cryoprotectant sample (i.e., ΔT_{fm} scaled down by a ratio of 20 to 35). It is noted that the typical uncertainty in thermocouple measurements is 0.5 °C, and that it is smaller than the maximum temperature difference along the cooling stage in most cases. In general, the authors of this paper find it somewhat surprising to have such small values of standard deviation in the fracture temperature, for any given set of experimental conditions. It is noted that the onset of fracturing is commonly considered to be a statistical event, especially in highly brittle materials. This observation may be very useful in modeling and predicting fracture formation in cryoprotectants.

The maximum temperature difference along the cooling stage, ΔT_{fm}, increased when substrates made of either glass or plastic were used, as a result of the introduction of contact resistance between the substrate on the heat exchanger. A common way of reducing contact resistance (which is mostly attributed to surface roughness and air voids between two solid surfaces) is by filling in the gaps with more highly conductive material, such as a commercial thermal grease, water, or even the cryoprotectant itself. However, such added material would freeze or vitrify at cryogenic temperatures, bonding the substrate to the heat exchanger, and thereby defeating the purpose of including a substrate material in the first place, as discussed in the continuum mechanics analysis section below.

A wide selection of images from the experiments summarized in Table 1 is available on a website published in conjunction with the current paper [25]. A representative selection of images from those experiments is presented in Figs. 3–8, where the fracture parameters associated with these experiments are listed in Table 2. Fig. 9 presents the thermal history of each of the samples presented in Figs. 3–7, calculated as the average temperature measurement by the four thermocouples of the cooling stage. It can be seen from Fig. 9 that the initial phase of cooling, at the maximum achievable rate

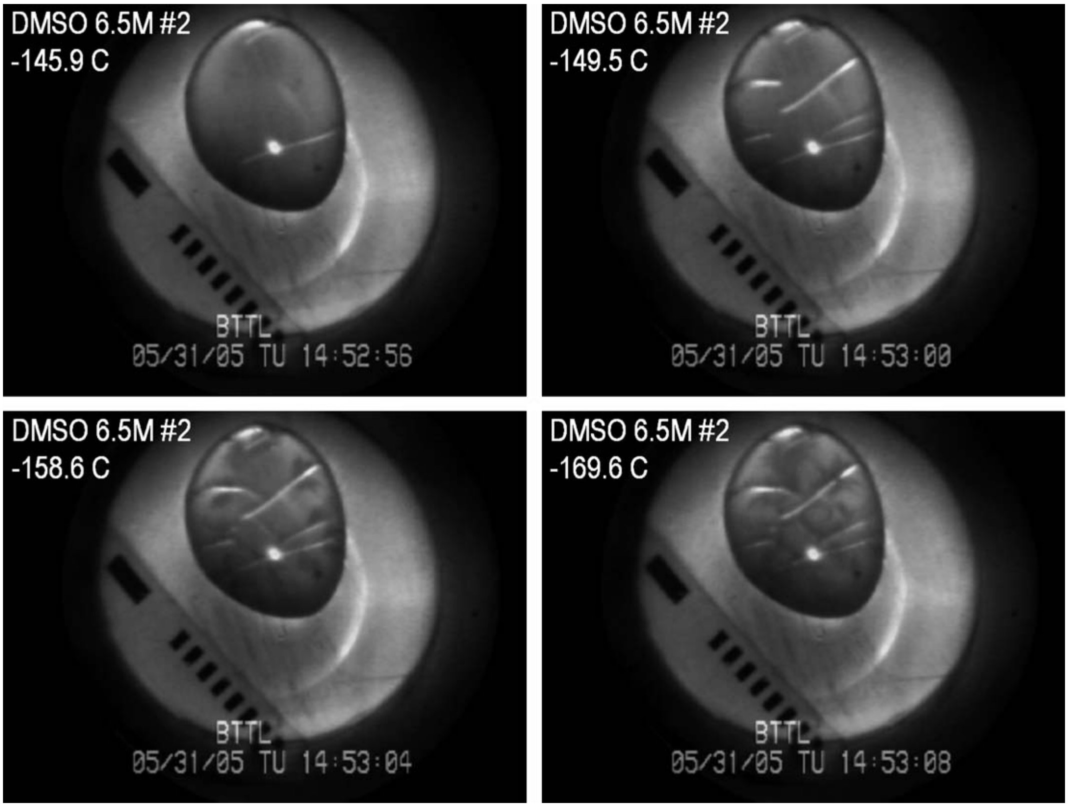

Fig. 3. Fracture formation in a vitrified 6.5 M DMSO sample on a copper base. The thermal history is presented in Fig. 9 and fracture parameters are listed in Table 2.

down to −120 °C, is very repeatable (when the main nitrogen valve is open, Fig. 1). It is further noted that cooling rate control with the needle valve, below −120 °C, is less repeatable than the cooling rate control in the initial stage of cooling.

Two values of cooling rates are listed in Table 2, H_1, which is the average cooling rate between −120 and −150 °C, and H_2, which is the average cooling rate at the onset of fracturing, calculated between $T_f - 10$ °C and $T_f + 10$ °C for each experiment. The observations that H_2 is greater than H_1 in many experiments (Table 2), and that the temperature of the sample does not decay exponentially with time to some steady state value (Fig. 9), may be counter intuitive if a simple convection regime is assumed in the channels of the cooling stage. If the heat transfer coefficient by convection in the channels is constant, and most of the cooling effect of liquid nitrogen is applied to cool the cooling stage, one could expect the system to behave like a lumped capacity system. Such a system is characterized by an exponential decay of temperature with time, down to the liquid nitrogen boiling temperature. However, heat transfer by boiling is a complex process, which goes through several regimes of boiling. The first regime is film boiling in the channels, which is the most inefficient regime for convective heat transfer during boiling, where a thin film of nitrogen gas always exists between the liquid nitrogen and the solid wall. The second phase of boiling is nucleate boiling, where progressively larger areas of the wall become wetted by liquid nitrogen. It is at that point where the cooling rate increases spontaneously. In the current experimental system, nucleate boiling starts to develop at about −150 °C.

It can be seen from Table 1 that the fracture temperature is not a strong function of the concentration of DMSO. For example, for experiments on a copper base in the absence of tissue segments, the difference between the average fracture temperature from all samples, and the average fracture temperature from a group of experiments with specific concentration, is less than one standard deviation in measurements from the same group. For a specific DMSO concentration, the difference in fracture temperature for samples in the presence and absence

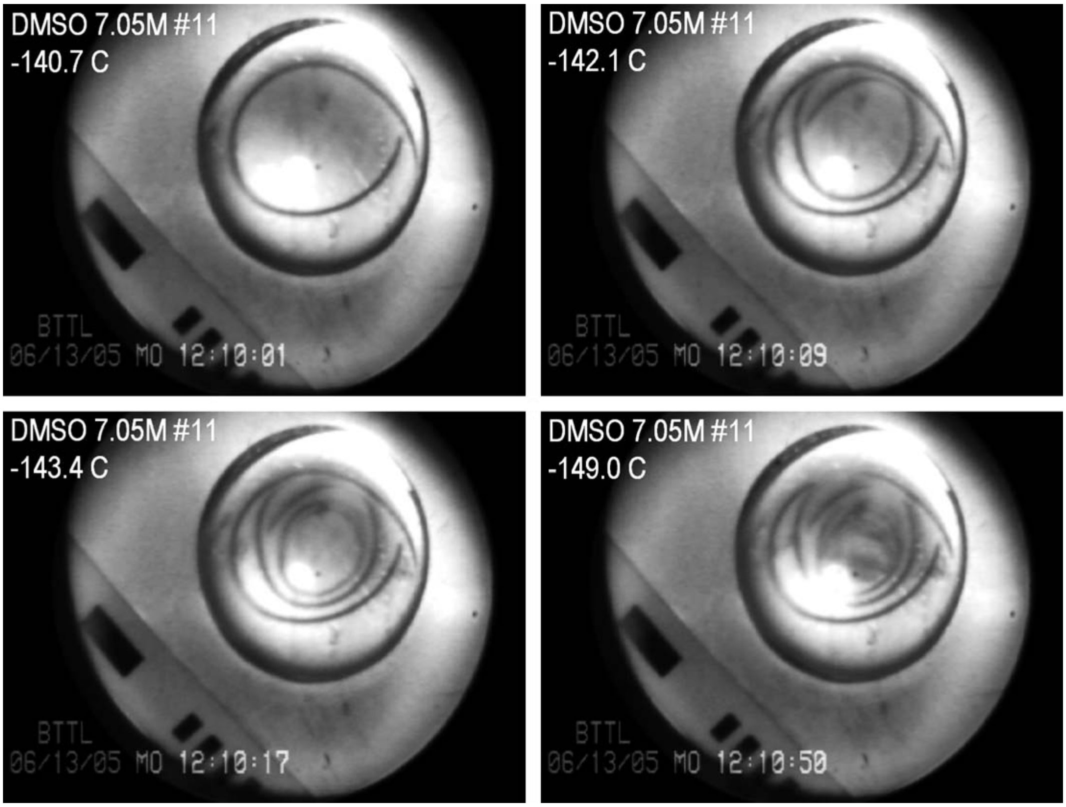

Fig. 4. Fracture formation in a vitrified 7.05 M DMSO sample on a copper base. The thermal history is presented in Fig. 9 and fracture parameters are listed in Table 2.

of tissue segments is less than two standard deviations in measurement, but with no definitive trend (a sample with tissue segments resulted in either lower or higher fracture temperature). This indicates an inconclusive effect of the presence of tissue segments on the fracture temperature.

It is noted that the standard deviation presented in Table 1 for any specific experimental conditions represents a wide variety of cooling rates. More cooling rate information is listed in the opening table on the associated website [25]. The effect of the cooling rates on the fracture temperature is discussed in more detail in the continuum mechanics analysis section.

It can be seen from Table 1 that the fracture temperature of VS55 and DP6 are comparable in the absence of tissue segments, and that on average it is about 8 °C above the fracture temperature of DMSO. Note that the glass transition temperature is −133.4 °C for 6 M DMSO [17], −132.0 °C for 7.05 M DMSO [17], −127.6 °C for 8.4 M DMSO [17], −123 °C for VS55 [14], and −119 °C for DP6 [26,31]. However, these glass transition values were obtained with a differential scanning calorimetry technique (DSC), with a standard protocol characterized by a low cooling rate of about 1 °C/min when approaching the glass transition temperature. Furthermore, these values represent the mid-point of glass transition upon rewarming (see Angell [1] for a review of common definitions for the glass transition temperatures), while the fracture temperature reported in the current study refers to the cooling phase only. In general, the glass transition during rewarming is expected to be at a higher temperature than the glass transition during cooling for the same material. Furthermore, the glass transition is expected to take place at a lower temperature for a higher cooling rate, where all the experiments of the current study were performed at higher cooling rates than those typically used in DSC measurements.

Fig. 3 presents results from a 6.5 M DMSO experiment at higher cooling rates. Two scales of fractures are observed here, long linear fractures, with a characteristic length similar to the radius of the droplet, and second generation fractures,

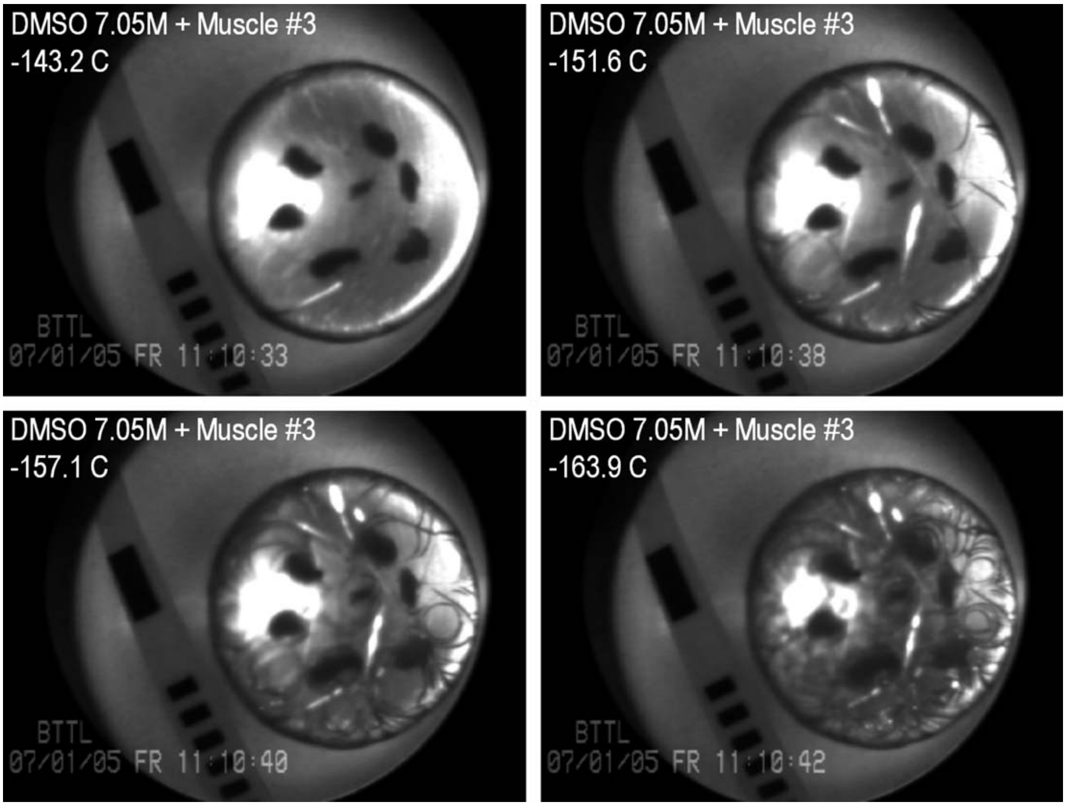

Fig. 5. Fracture formation in a vitrified 7.05 M DMSO sample containing seven bovine muscle segments on a copper base. The thermal history is presented in Fig. 9 and fracture parameters are listed in Table 2.

extending from the main fractures, having an order of magnitude shorter characteristic length. Note that the maximum cooling rate achievable by the current heat exchanger setup (∼100 °C/min) was not fast enough to vitrify 6 M DMSO.

Fig. 4 presents results from a 7.05 M DMSO experiment at lower cooling rates. Fractures here are circular, with the first fracture always occurring at a larger diameter. Fracture formation progresses in a similar pattern to smaller radii as the temperature decreases. Comparable results were obtained in many low cooling rate DMSO experiments.

Fig. 5 presents results typical of DMSO at 7.05 M or higher concentrations, when subject to high cooling rates. The initial development of fractures may appear random, but progressive fracturing creates imaginary "cells", where the typical cell diameter decreases with the decrease in temperature. (The pattern is akin to mud cracking or cracking in ceramic glazes. The progressive shrinking in the cell size with temperature is akin to the reduction in linear crack spacing in thin films bonded to ductile substrates as strain increases [3]). No relationship between the bovine muscle tissue segments and the pattern of fractures is demonstrated in Fig. 5.

Fig. 6 presents results from an 8 M DMSO experiment at low cooling rates in the presence of tissue segments. It can be seen from Fig. 8 that the first fracture occurred at a larger radius than the location of the tissue segment, in a pattern resembling the first fracture in Fig. 4. The effect of the tissue segments becomes noticeable only when fractures continue to develop at smaller radii. Then, it appears that the fractures are being either initiated at or arrested by the tissue segments. Note how the tips of the fractures are diverted inward, towards the tissue segments, rather than continuing on roughly the same radius. As the cooling process progresses, more and more fractures develop perpendicular to the initial circular fracture, first at larger radii, and eventually populating the entire sample.

Fig. 7 presents results from an 8.4 M DMSO experiment at low cooling rates, in the presence of tissue segments. It appears that the tissue segments in this case are responsible for the specific pattern

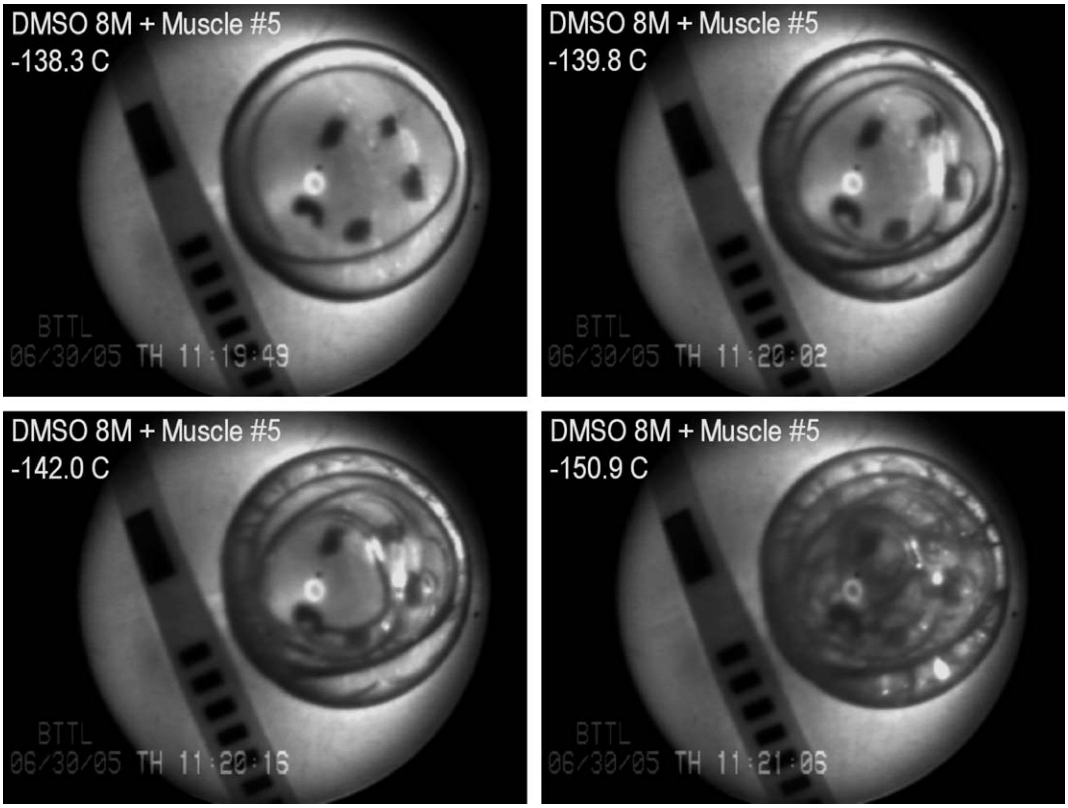

Fig. 6. Fracture formation in a vitrified 8 M DMSO sample containing five bovine muscle segments on a copper base. The thermal history is presented in Fig. 9 and fracture parameters are listed in Table 2.

of fracturing, where fractures are likely to be initiated or arrested at all five segments. No circular pattern of fracturing is observed in this experiment. Despite the similar conditions of the experiments presented in Figs. 6 and 7 (see also Table 2 and Fig. 9), the fracturing pattern is distinctly different, yet the fracture temperature deviates by only 1.3 °C.

It can be concluded from Figs. 5–7, as well as from other experiments with tissue segments, that the presence of these tissue segments does not change significantly the fracture temperature. However, once fractures start to develop, the pattern of fracture formation is definitely affected by the presence of tissue segments.

Fig. 8 provides four snapshots of various effects in VS55 and DP6. Partial crystallization is observed in the top two images: VS55 on the top-left and DP6 on the top-right. Crystals appear as darker spots in the transparent surroundings near the edge of the DP6 sample. The center of the DP6 samples appears completely opaque, with significantly more crystals. No fractures can be observed in the DP6 sample. Ice crystals are a bit more difficult to observe in the VS55 sample (more evident near the top-left of the sample). Four tissue segments are even more difficult to observe in that image, due to partial cryoprotectant crystallization. The partially crystallized VS55 sample shows a significant number of fractures.

The bottom images in Fig. 8 present fracture formation in VS55 on a glass substrate, having a thickness of 1 mm (bottom-left) and 150 μm (bottom-right). The glass substrate is square; as a result the cryoprotectant droplet is typically not as circular as in the experiments shown in Figs. 3–7, and the resulting fractures pattern is typically non-circular. Fractures on glass tend to form polygonal fracture cells, rather than the circular cells, as shown in Fig. 5 for example. In general, and as can be seen from Table 1, the presence of glass substrates reduces the fracture temperature. A thinner glass substrate reduces the fracture temperature more than a thicker glass substrate. The presence of a 120 μm plastic substrate reduces the fracture temperature further, and eliminates them altogether for VS55. However, results are not as conclusive for 30 μm

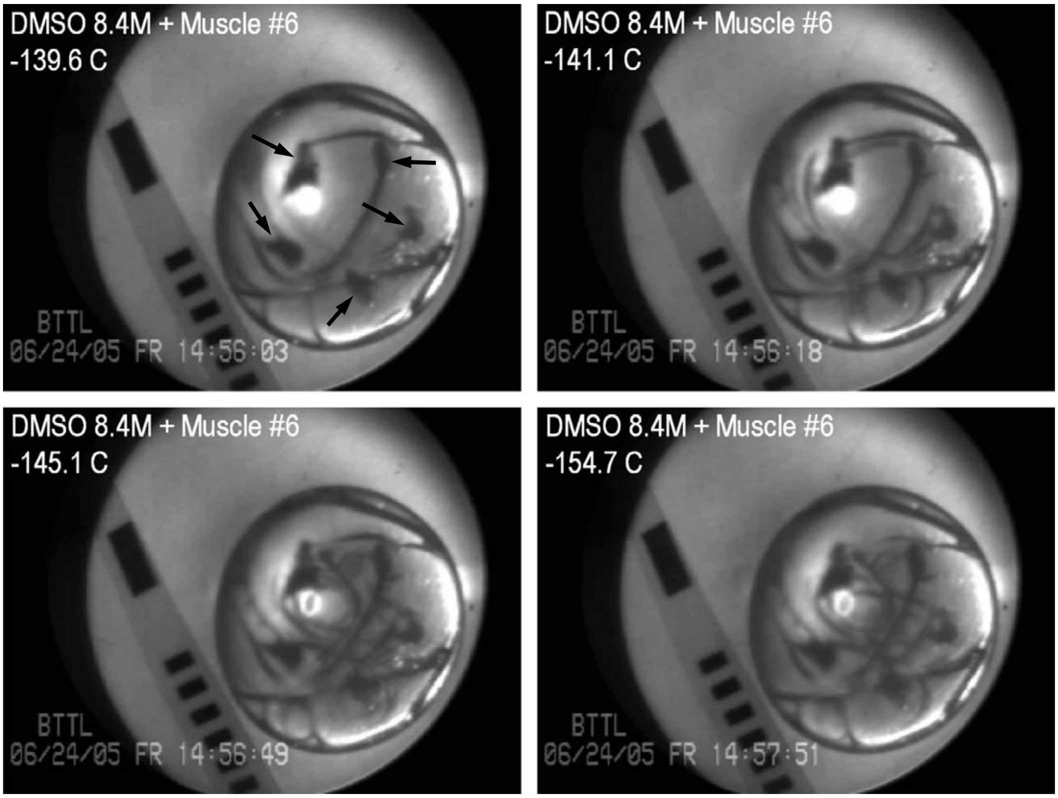

Fig. 7. Fracture formation in a vitrified 8.4 M DMSO sample containing five bovine muscle segments (indicated by arrows) on a copper base. The thermal history is presented in Fig. 9 and fracture parameters are listed in Table 2.

plastic substrates, and it is likely to be associated with difficulties in sample handling under those conditions. Results from the 30 μm plastic substrate define the limitation of the current experimental work in terms of substrate thickness.

Finally, the experimental setup is designed to study fractures in thin films, where the diameter of the droplet is an order of magnitude greater than its thickness. While an effort was made to make the droplet contour perfectly circular, variation from the circular shape can be observed in Figs. 3–8 and in the companion images [25]. The observation that the temperature to fracture is found in a narrow range for imperfectly circular droplets suggests that the droplet behaves like a thin film in the continuum mechanics sense, where end effects are not dominant. Furthermore, while the pattern of fracturing may be affected by the shape of the droplet, the presence of uniformly distributed "cells" of fracture in some figures (Fig. 5 for example) also supports the interpretation that the droplet behaves like a thin film; here, the diameter of the cell is proportional to the propagation distance of end effects. These observations serve as key elements in the continuum mechanics modeling in the next section.

Continuum mechanics analysis

The objective in this section is to combine thermal stress analysis with experimental results, to study whether fractures are consistent with thermal stresses predicted during vitrification. These mathematical results will be used as building blocks for prediction of continuum mechanics effects in future studies, in more complex geometries, and subject to a variety of thermal conditions. The mechanism of stress development for a droplet adhering to a substrate has been presented in [31]. The droplet deforms due to temperature changes and due to stress (tension); stress produces both elastic deformation and viscous (creep) deformation. The usual assumption is adopted that elastic, viscous, and thermal contributions to strain superpose [13]. The total tensile strain-rate $\dot{\varepsilon}$ under conditions of uniaxial stress is

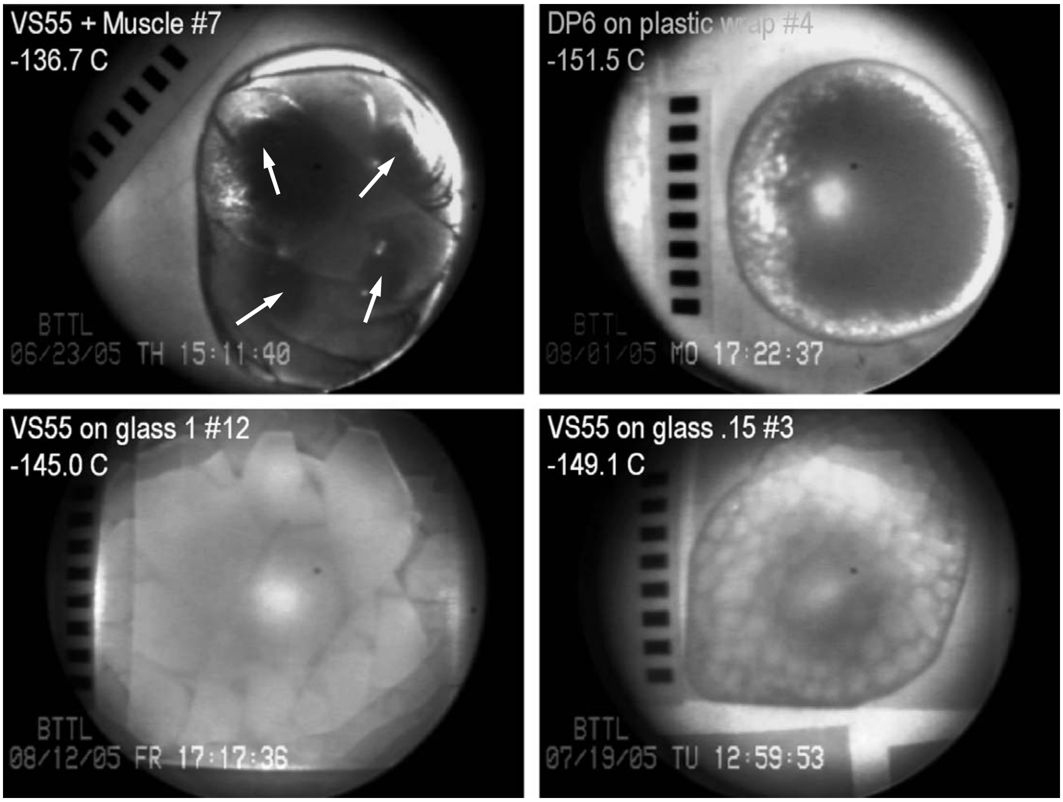

Fig. 8. (Top-left) fracture formation in a partially vitrified VS55 sample containing four bovine muscle segments (indicated by arrows) on a copper base. (Top-right) a partially vitrified DP6 sample on a 30 μm plastic substrate. (Bottom-left) fracture formation in a vitrified VS55 sample on a 1 mm glass substrate. (Bottom-right) fracture formation in a vitrified VS55 sample on a 150 μm glass substrate.

Table 2
Summary of results for the experiments presented in Figs. 3–9, where T_f is the fracture temperature, ΔT_{fs} is the estimated variation of temperature along the sample, H_1 is the cooling rate between −120 and −150 °C, and H_2 is the cooling rate between $T_f - 10$ and $T_f + 10$ °C

Experiment No.	Cryoprotectant	Muscle segments	Substrate	T_f, °C	ΔT_{fs}, °C	H_1, °C/min	H_2, °C/min
2 (Fig. 3)	6.5 M DMSO	–	Copper	−145.9	1.5	35.9	44.8
11 (Fig. 4)	7.05 M DMSO	–	Copper	−139.6	1.3	6.2	7.7
3 (Fig. 5)	7.05 M DMSO	+	Copper	−143.2	3.1	47.8	61.2
8 (Fig. 6)	8 M DMSO	+	Copper	−138.3	0.6	5.4	8.1
6 (Fig. 7)	8.4 M DMSO	+	Copper	−139.6	0.4	4.8	6.6
7 (Fig. 9)	VS55	+	Copper	−136.7	2.6	55.9	50.0
4 (Fig. 9)	DP6	–	30 μm Plastic	None	N/A	100.3	N/A
12 (Fig. 9)	VS55	–	1 mm Glass	−126.2	3.4	77.7	57.4
3 (Fig. 9)	VS55	–	150 μm Glass	−152.7	4.1	49.5	27.5

then the sum of the elastic strain-rate, the viscous strain-rate, and the thermal strain-rate:

$$\dot{\varepsilon} = \frac{1}{E}\frac{d\sigma}{dt} + \frac{\sigma}{3\eta} + \beta\frac{dT}{dt} \quad (1)$$

where σ is the tensile stress, E is the elastic modulus, η is the shear viscosity, and β is the coefficient of thermal expansion. The elastic and thermal contributions may be more familiar in the forms $\varepsilon_{\text{elastic}} = \sigma/E$ and $\varepsilon_{\text{thermal}} = \beta\Delta T$, which are differentiated with time in Eq. (1). The material is assumed to respond isotropically; consequently, the elongational viscosity is three times the shear viscosity, which explains the factor of 3 in the denominator of Eq. (1). The thermal strain rate is significant at all temperatures. The elastic modulus is essentially

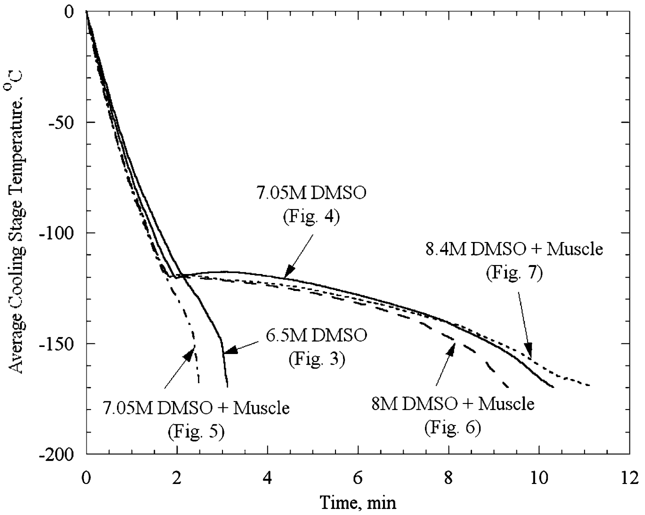

Fig. 9. Thermal history of the experiments shown in Figs. 3–7. The fracturing parameters associated with these experiments are listed in Table 2.

constant with temperature, while the viscosity increases by orders of magnitude; thus, the viscous strain rate is important at high temperatures and unimportant at low temperatures.

Two different methods of solution are used to compute the stress in the CPA in the current study. The first ignores the influence of deformations due to stress on the substrate entirely, and is applicable to the case of a thick substrate, such as the copper heat exchanger. Here, the stress in the circular droplet of the cryoprotectant is approximated as uniform (which is nearly true except for the edges). The tensile stresses in the plane of the sample are equal in all directions, and the stress perpendicular to the sample is zero. Given the thermal history of the sample, the stress can be found by time integration of the following equation [13]:

$$\frac{1-v}{E}\frac{\mathrm{d}\sigma}{\mathrm{d}t}+\frac{\sigma}{6\eta}+\beta_{\mathrm{CPA}}\frac{\mathrm{d}T}{\mathrm{d}t}=\beta_{\mathrm{Substrate}}\frac{\mathrm{d}T}{\mathrm{d}t} \tag{2}$$

The Poisson ratio, v, of the CPA, and the extra factor of 1/2 in the viscous strain-rate term enter to account for stress acting in all directions in the plane of the sample (see Appendix A for more details). The integration must account for the temperature dependency of both the viscosity and the thermal expansion.

In the second method, a finite element numerical technique (ANSYS 8.1) is used, and the deformation and stress in both the droplet and the substrate are computed. This method is required when the substrate is thin, and the overall force applied by the CPA to the substrate is high enough to bend the substrate. Here, the CPA is still modeled with Eq. (1), but the substrate is modeled as a linear elastic material. The domain (shown in the inset in Fig. 13) consists of a circular disk of CPA bonded to a circular disk of substrate, with zero forces on their outer surfaces. The mesh for the case of the sample on copper is modeled with 8-noded axi-symmetric Plane183 elements, 400 in the droplet, and 250 in the copper. To include the functional dependencies of viscosity on temperature discussed below, a special purpose user-defined creep function was employed. To facilitate the time integration, the viscosity was set not to fall below 1.9×10^{8} Pa-s at high temperatures, and not to exceed 10^{20} Pa-s at low temperatures. These limits were determined to have minimal impact on the numerical results.

Typical physical properties of the CPA and the substrate are listed in Table 3. The elastic moduli of cryoprotectants are unknown, and a value of 1 GPa has been selected for the current study, which is typical of organic materials. The implication of this choice on the results is straightforward, as explained below.

The viscosity of DMSO at various molar concentrations has been measured in the temperature range of 20 to −45 °C with falling ball viscometry [29]; the authors are unaware of viscosity measurements of DMSO at lower temperatures, or of VS55 and DP6 at all. Moreover, the viscosity of DMSO in the temperature range of interest (in the vicinity of

Table 3
Typical physical properties for the CPA and substrate

	$\beta \times 10^6$, °C^{-1}	ν	E, GPa
Copper	17 [8]	0.33 [8]	120 [8]
Glass	4 [4]	0.2 [4]	70 [4]
Plastic	20 .. 80 [9]	0.4 [9]	2..4 [9]
VS55	0.4024 T + 184.1 [23]	0.2*	1**
DP6	0.7798 T + 193.5 [23]	0.2*	1**
7.05 M DMSO	0.5634 T + 208.4 [23]	0.2*	1**

* Typical value for brittle materials [28].
** Typical value for organic materials [2].

glass transition) is orders of magnitude higher than that in the range of available experimental data [29]. While T_g is commonly measured with differential calorimetry techniques (DSC), an alternative definition of glass transition is the temperature at which the viscosity reaches 10^{12} Pa-s (10^{13} Poise). In the absence of viscosity data at low temperatures, the following functional behavior is assumed [29]:

$$\eta(T) = \eta_0 \exp\left(\frac{b}{T - T_0}\right)[Pa - s];$$
$$\eta_0 = 10^{12} \exp\left(\frac{-b}{T_g - T_0}\right) \qquad (3)$$

Eq. (3) yields a viscosity value of 10^{12} Pa-s at the glass transition temperature (measured with DSC), and the parameters T_0 and b are chosen to fit to the available experimental data at higher temperatures [29].

Mathematical results and comparison with experimental observations

Variation of stress with temperature

Typical stress results in the droplet as a function of temperature are shown in Fig. 10, which displays the case of DMSO on copper subject to a constant cooling rate of 5 °C/min. The viscosity function presented in Eq. (3), with $b = 8.607$, $T_0 = -162.1$ °C, and $T_g = -132$ °C, best fit the experimental data at high temperatures [29] and is designated as the baseline viscosity. The CPA tends to shrink with cooling at a higher rate than the substrate, because of the difference in thermal expansions. Due to adherence, however, the substrate seeks to prevent the CPA from shrinking by applying stress to it. When the temperature is high and the viscosity of the CPA is low, creep deformation can readily compensate for the thermal mismatch with very low stresses. As the temperature decreases and the CPA viscosity increases, compensating for the mismatch requires higher stresses, which now produce creep and elastic deformation of comparable magnitude. If the cooling rate is decreased, then the compensating strain-rate due to stresses is lower, and the material can be cooled to lower temperatures before stresses become significant. Eventually, the CPA responds like an elastic solid: the stress increase at low temperatures depends on the difference in the thermal expansions and on the elastic properties

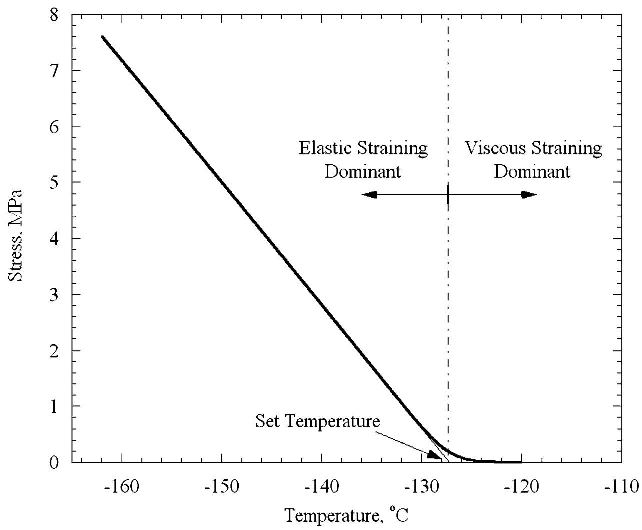

Fig. 10. Typical stress results in a DMSO droplet vitrified directly on the copper heat exchanger, subject to a constant cooling rate of 5 °C/min.

of the CPA. For practical purposes however, the build-up in stress only begins below some temperature threshold. We define a "set-temperature" (Fig. 10) as the extrapolation of the linear portion of the theoretically computed stress vs. temperature curve to zero stress. As discussed further below, the set temperature inferred from the calculations will depend on the variation of CPA viscosity with temperature.

From the observed temperature of fracture, one can infer the apparent fracture stress from the curve presented in Fig. 10. For the parameters used to generate that curve, the fracture stress corresponding to the mean temperature of cracking for 7.05 DMSO with no tissue, $T_f = -141.7$ °C (Table 1), is 3.2 MPa. If the elastic modulus had been different (since $E = 1$ GPa was merely a guess), the stress would have changed nearly in proportion. However, the ratio of the stress at fracture to the elastic modulus, also defined as the fracture strain, is essentially independent of the choice of elastic modulus value. Note that a fracture strain of 0.0032, deduced from the above calculations for 7.05 M DMSO, is within the range of values typical of brittle plastics.

Dependence on viscosity

Since the variation of viscosity at low temperatures is uncertain, the sensitivity of the predicted stress to the viscosity is of interest. Several viscosity functions were investigated, as presented in Fig. 11, and predictions for the resulting stress are plotted in Fig. 12, all for 7.05 M DMSO on copper subject to a cooling rate of 5 °C/min. It can be seen from Fig. 12 that only the set temperature varies between the different viscosity cases, where the linear portion of each curve is associated with the same elastic modulus and thermal expansion. Since the stress remains practically zero down to about 10 °C above T_g, the shape of the viscosity function is significant only near T_g. Moreover, the set temperature decreases with increase in the slope of the viscosity near T_g (values are listed in Fig. 12). If one discounts the rather implausible curve, identified with "*" in Fig. 12 (representing a linear variation of logarithm(viscosity) with decreasing temperature, rather than an exponential function), then the set temperature might vary over a range of 3.5 °C. Therefore, the fracture strain of 7.05 M DMSO is likely to range from 0.28% to 0.36%.

Dependence on cooling rate

To study the cooling rate effect on the developing stress, Eq. (2) was solved again for the best fit viscosity curve illustrated in Fig. 11, over a cooling rate range of 0.5–500 °C/min. If one presumes that fracture occurs at a fixed stress, independent of the strain rate, one can predict the variation of fracture temperature with cooling rate. The fracture

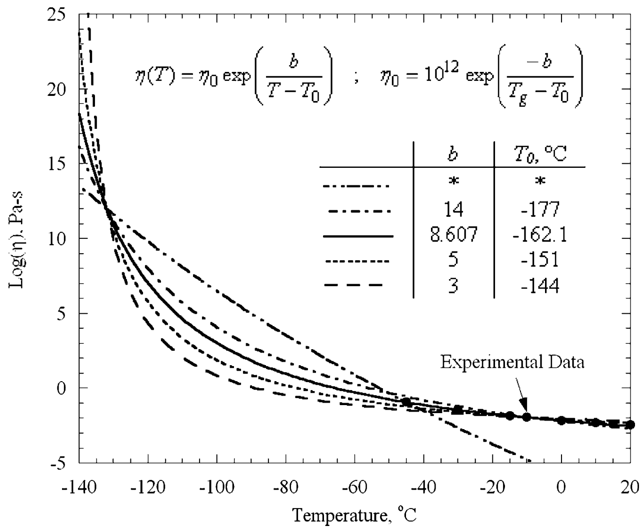

Fig. 11. Assumed dependency of viscosity on temperature for the purpose of parametric studies in 7.05 M DMSO ($T_g = -132$ C). The functional behavior and parameters are shown in the figure, except for the extreme case marked with "*", which is modeled as $\eta = 1.234 \times 10^{145}\ (T)^{-61.95}$. The solid line represents the best fit with experimental data.

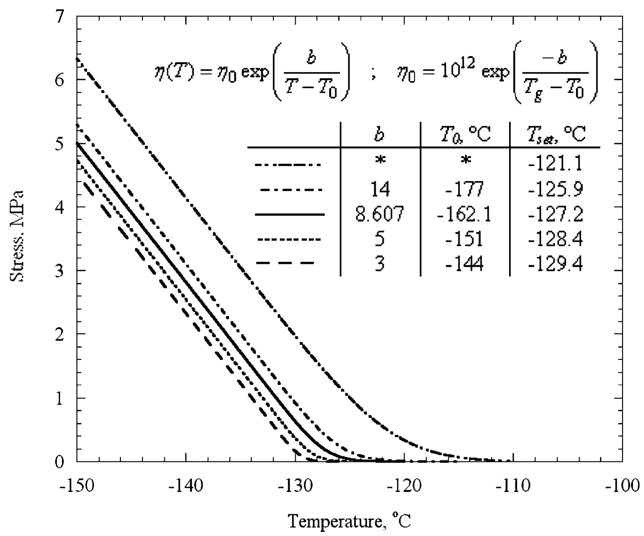

Fig. 12. Predicted stress versus temperature at a cooling rate of 5 °C/min, for a 7.05 M DMSO film, and for the various viscosity functions presented in Fig. 11.

temperatures for various cooling rates listed in Table 4 are based on the observed fracture temperature of −142 °C, which was taken to correspond to a cooling rate of 5 °C/min. The set temperature is also given in Table 4; since the set temperature is based on extrapolating the linear stress versus temperature down to zero stress, the difference between fracture temperatures at two cooling rates is equal to the difference between their respective set temperatures. It can be seen that the fracture temperature increases by only 7.2 °C as the cooling rate increases by three orders of magnitude; 0.5 and 500 °C/min bound the practical cooling rates for cryopreservation via vitrification. The modest variation in fracture temperature with large changes in cooling rate that is predicted is consistent with the lack of any systematic variation over the more limited ranges of cooling rates achieved in the experimental results reported here.

Table 4
Predicted set temperatures, T_{set}, fracture temperatures, T_{frac}, and derivative of viscosity with respect to temperature, for various cooling rates

H, °C/min	T_{set}, °C	T_{frac}, °C	$\lvert d\eta/dT \rvert$, Pa-s/°C	R
0.5	−129.2	−144.1	$3.73 \cdot 10^{10}$	1.49
5	−127.1	−142.0	$3.66 \cdot 10^{9}$	1.46
50	−124.7	−139.6	$3.55 \cdot 10^{8}$	1.42
500	−122.0	−136.9	$3.48 \cdot 10^{7}$	1.39

The parameter R is defined in Eq. (7), and is associated with the set temperature.

A simple argument is now presented to estimate the set temperature, and to rationalize the stress dependence on cooling rate. For high temperatures, the elastic contribution is negligible, and the first term in Eq. (2) can be neglected. For a constant cooling rate and thermal expansion coefficient, Eq. (2) can be rearranged to estimate the increase in stress with time:

$$\frac{d\sigma}{dt} = 6\frac{d\eta}{dt}\left[(\beta_{\text{Substrate}} - \beta_{\text{CPA}})\frac{dT}{dt}\right] \tag{4}$$

For low temperatures, by contrast, the viscous contribution [second term in Eq. (2)] is negligible, and Eq. (2) can be rearranged to estimate the increase in stress with time:

$$\frac{d\sigma}{dt} = \frac{E}{1 - v}\left[(\beta_{\text{Substrate}} - \beta_{\text{CPA}})\frac{dT}{dt}\right] \tag{5}$$

The set temperature can be viewed as the temperature where the material response transitions from viscous dominated to elastic dominated. This should take place when the estimates from Eqs. (4) and (5) are comparable, that is:

$$\frac{E}{1 - v} \approx 6\frac{d\eta}{dt} = 6\frac{d\eta}{dT}\frac{dT}{dt} \tag{6}$$

With E, v, and dT/dt remaining constant, and η varying smoothly with temperature, Eq. (6) implicitly defines a single temperature, which we argue should be close to the set temperature inferred from extrapolating the numerical results, as described above.

To test this relation, we extracted the set temperature from the numerical results of integrating Eq. (2), and then computed $d\eta/dT$ at this temperature from the viscosity function (Fig. 11). The ratio of the right term to the left term of Eq. (6) can be rearranged in the form:

$$R \equiv \left(6\frac{d\eta}{dT}\frac{dT}{dt}\right)\Big/\left(\frac{E}{1-v}\right) = \left[\frac{-6\eta_0 b}{(T-T_0)^2}\exp\left(\frac{b}{T-T_0}\right)\frac{dT}{dt}\right]\Big/\left(\frac{E}{1-v}\right) \qquad (7)$$

It can be seen from Table 4 that R at T equal to the set temperature is $1.44 \pm 3.5\%$ for cooling rates varying over three orders of magnitude, which confirms the explanation for the determinants of the set temperature. Moreover, one now has a simple way of estimating the set temperature: given values of cooling rate and elastic modulus, the set temperature satisfies Eq. (7). The set temperature is seen to be relatively insensitive to elastic modulus and to cooling rate: To keep the ratio R constant with even a substantial change in cooling rate requires only a small change in the set temperature, because the viscosity function is so dramatically dependent on temperature.

Dependence on substrate

To provide additional evidence that cracking is indeed tied to thermal stress and not to temperature per se, droplets of CPA were cooled on substrates that were placed upon, but not bonded to, the copper heat exchanger. As discussed above, fracture temperature was indeed observed to change significantly as the substrate was changed. Finite element calculations were conducted to determine the stress in the CPA associated with different substrates. Fig. 13 presents the variation in the circumferential stress through the droplet thickness along its center line, at −142 °C, for different substrate conditions (in the absence of a more specific data, two extreme sets of thermoelastic parameters for the plastic were chosen). In the case of the copper, the prediction based on Eq. (2) and the finite element calculations are essentially the same. The elastic deformation of the copper is negligible, and thermal strain of copper dictates that of the CPA. For the cases of the thin glass and plastic substrates, the stress in the CPA varies from tensile at the substrate surface to compressive (negative) on the free surface.

Besides the important effect of the thermal expansion difference between the CPA and the substrate, these results indicate that lower levels of stress are produced when the substrate is more flexible, either by being thinner or having a lower elastic modulus. Greater flexibility means less resistance to the contraction of the CPA and hence lower stress. While precise predictions of the actual temperature to fracture with such non-uniform stress distributions requires much additional work, the general trend of diminished stress for the different substrates

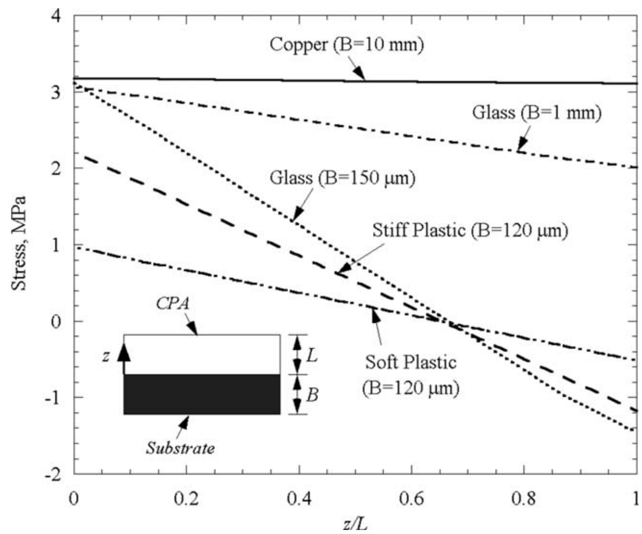

Fig. 13. Predicted stress across the droplet thickness, along its center-line, for various substrates, for a cooling rate of 5 °C/min and best fit viscosity (Fig. 11). The thickness of the droplet, L, is 1.5 mm.

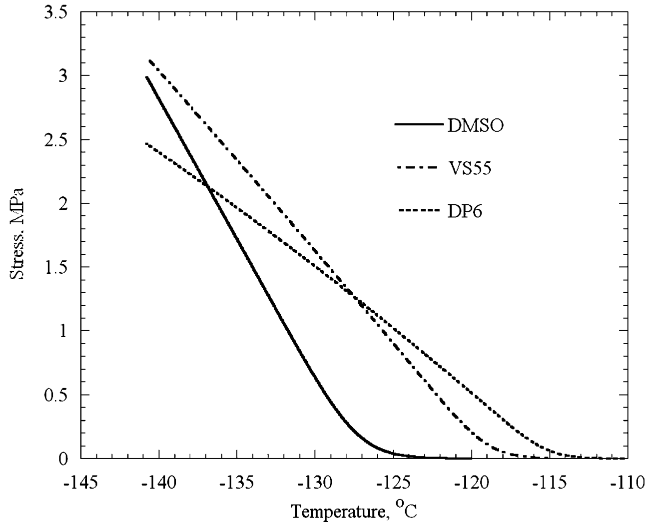

Fig. 14. Predicted circumferential stress for different cryoprotectants vitrified directly on the copper heat exchanger, subject to a cooling rate of 5 °C/min; viscosities of VS55 and DP6 fit to their T_g and to viscosity of DMSO at higher temperatures.

is consistent with the observed decrease in fracture temperatures, supporting the hypothesis that thermal stress governs fracture.

Results for VS55 and DP6

Calculations were also carried out for stresses in VS55 and DP6 vitrified on copper, using viscosity functions which best fit the measured values of T_g (-123 °C and -119 °C, respectively) and experimental data for DMSO at higher temperatures (in the absence of specific viscosity data for these cocktails). The same elastic modulus of 1 GPa was presumed. Comparison with the stress in DMSO is shown in Fig. 14. As expected, the set temperature increases as T_g increases. The different slopes reflect the different thermal expansion coefficients. Using the observed mean fracture temperatures, one infers a fracture strain in VS55 and DP6 of 0.23% and 0.18%. These are also in the range of brittle organic materials, but somewhat lower than that of pure DMSO, as discussed above. There is somewhat less certainty in these predictions, given the lower certainty in viscosity. Nevertheless, inferences as to the failure strains in these other cryoprotectants are proving useful in ongoing studies of fracture.

Summary and conclusions

Fracture formation in thin films of vitrified cryoprotectants has been investigated experimentally, and concepts from the theory of continuum mechanics were applied to explain the experimental observations.

Experimental results show that the onset of fracturing in vitrified films of cryoprotectants is very consistent, occurring over a small temperature range. This observation is a bit surprising to the authors of this paper, and it will have a direct impact on future continuum mechanical analyses of cryopreservation.

For DMSO in the concentration range of 6.5 and 8.4 M, the onset of fracture was found to be insensitive to the concentration. The fracture pattern, however, varied between different DMSO concentrations, once fracturing started to progress. Experimental results indicate that the onset temperature of fracture, as well as the intensity of fracture propagation, decreased with the decrease in stiffness of the substrate carrying the cryoprotectant sample. This evidence further solidifies the hypothesis that fracture is driven by thermal stress not with temperature per se.

Fracture pattern was also affected by the cooling rate. At low cooling rate, initial fractures were found to be long and circular, with the first fracture always occurring at a larger diameter. Fracture formation progressed in a similar pattern to smaller radii as the temperature decreases. At high cooling rates, the initial development of fractures appeared random, but progressive fracturing formed imaginary circles or cells, where the typical diameter of the cell decreases with the decrease in temperature.

The presence of small tissue segments appeared not to affect the onset temperature of fracturing. The effect of the tissue segments becomes noticeable only when fractures continue to develop. Then, it appeared that fractures are initiated at, or arrested by, the tissue segments.

From continuum mechanics analysis, a simple picture of stress development in cryoprotectant droplets vitrified on substrates has emerged. With cooling, the stress is nearly zero until a "set" temperature is reached; the stress builds up linearly thereafter with diminishing temperature. The set temperature, which is on the order of 5–10 °C above T_g, is determined principally by how rapidly the viscosity increases with temperature near T_g. Viscosity as a function of temperature for DMSO was approximated by fixing it to 10^{12} Pa-s at T_g and fitting to experimental data for temperatures in the range of 20 to −45 °C. Stresses were predicted for the best fit viscosity and for other viscosity functions having milder and sharper variations with temperature. From the observed temperature to fracture, one can infer the stress or strain at fracture; strains to cause fracture in DMSO are likely to be in the range of 0.28–0.36%, typical of brittle organic materials.

The reasonableness of predicted values of fracture strain supports the thermal stress theory for the origin of cracking in vitrified CPA. Additional evidence for this explanation of cracking is provided by observations of diminished cracking tendency on thin substrates. Stress analyses confirm that the stress in the CPA is markedly less when the cooling occurs on a thin substrate that can bend and not fully restrain the contracting CPA. Analyses also shed light on the effect of cooling rate: the fracture temperature is predicted to increase by approximately 2 °C with every decade increase in cooling rate. Predictions of stress were likewise made for VS55 and DP6 (using the T_g for those CPAs and high temperature viscosity data for DMSO); comparisons with fracture temperature place the fracture strains at 0.23% and 0.18%, respectively.

In general, vitrifying CPA in contact with a material with much lower thermal expansion leads to stress and cracking, even if the temperatures are uniform, as studied here. Temperature gradients within CPA or tissue are another mechanism whereby stresses are generated; such gradients are likely to be a factor when vitrifying not thin layers but more bulky specimens. Such issues are also worthy of closer investigation.

Acknowledgments

This study has been supported in part by NHLBI, Grant No. R01 HL069944. The authors thank Mr. Jim Dillinger, Mr. John Fulmer, and Mr. Edward Wojciechowski, of the Machine Shop, Department of Mechanical Engineering, Carnegie Mellon University, Pittsburgh, PA, for assistance in constructing the experimental apparatus. The authors thank Dr. Michael J. Taylor, Cell and Tissue Systems, Inc., Charleston, SC, for the insightful discussions about the application of cryoprotectants.

Appendix A

The approximate solution for stresses in the axisymmetric droplet, presented in Eq. (2), is based on a uniform stress state of $\sigma_r = \sigma_\theta \equiv \sigma$ in the r and z-directions, and $\sigma_z = \tau_r = 0$. This stress state satisfies the stress equations of equilibrium precisely, and the boundary condition of zero force ($\sigma_z = \tau_{rz} = 0$) on the upper surface. It does not satisfy the zero force condition on the outer edge; however, this simplified solution approximates the complete solution to a high degree of accuracy several thicknesses away from the free edge. Indeed, the finite element analysis, which makes no assumption on the thinness of the layer, confirms that this stress state is reached away from the edge. (In the complete solution, the tension is transferred to the droplet by shear stresses exerted by substrate over a small zone of contact near the outer edge.) Furthermore, the uniform stress state gives rise to uniform compatible strains that are consistent with the substrate, if the substrate contracts uniformly under the presumed uniform temperature, and if the substrate deformation due to stress is neglected.

With an isotropic elastic response, the elastic strains reduce to:

$$\varepsilon_{r,\mathrm{elastic}} = \frac{\sigma_r - v(\sigma_\theta + \sigma_z)}{E} = \frac{(1-v)\sigma}{E} \tag{A.1}$$

$$\varepsilon_{\theta,\mathrm{elastic}} = \frac{\sigma_\theta - v(\sigma_r + \sigma_z)}{E} = \frac{(1-v)\sigma}{E} \tag{A.2}$$

With an isotropic viscous response, viscous strains are associated with shear stresses or, in the general case, with deviatoric stresses (s_r and s_θ), which are defined as the actual stress components minus the hydrostatic part of the stress:

$$\dot{\varepsilon}_{r,\mathrm{viscous}} = \frac{s_r}{2\eta} = \frac{\sigma_r - 1/3(\sigma_r + \sigma_\theta + \sigma_z)}{2\eta} \tag{A.3}$$

$$\dot{\varepsilon}_{\theta,\mathrm{viscous}} = \frac{s_\theta}{2\eta} = \frac{\sigma_\theta - 1/3(\sigma_r + \sigma_\theta + \sigma_z)}{2\eta} \tag{A.4}$$

Using the simplified stresses, one finds:

$$\dot{\varepsilon}_{\theta,\mathrm{viscous}} = \dot{\varepsilon}_{r,\mathrm{viscous}} = \frac{\sigma}{6\eta} \tag{A.5}$$

References

[1] C.A. Angell, in: K.H.J. Buschow, R. Cahn, M.C. Flemings, B. Ilschner, E.J. Kramer, S. Mahajan (Eds.), Encyclopedia of Materials: Science and Technology, Chapter 4, Elsevier, New York, 2001, pp. 3565–3575.

[2] M.F. Ashby, D.R.H. Jones, Engineering Materials: An Introduction to their Properties and Applications, Pergamon Press, Oxford, 1980.

[3] B.F. Chen, J. Hwang, G.P. Yu, J.-H. Huang, In situ observation of the cracking behavior of TiN coating on 304 stainless steel subjected to tensile strain, Thin Solid Films 352 (1999) 173–178.

[4] Corning Inc., Acton, MA (supplier data).

[5] B.H. Dennis, G.S. Dulikravich, Y. Rabin, Optimization of organ freezing protocols with specified allowable thermal stress levels, in: IMECE 2000, Orlando, FL, November 5–10, ASME HTD-Vol. 368/BED-Vol. 47, 2000, pp. 33–48.

[6] G.M. Fahy, J. Saur, J.R. Williams, Physical problems with the vitrification of large biological systems, Cryobiology 27 (1980) 492–510.

[7] G.M. Fahy, Biological effects of vitrification and devitrification, in: D.E. Pegg, A.M. KarowJr. (Eds.), The Biophysics of Organ Preservation, Plenum Publishing Corp., New York, 1987, pp. 265–297.

[8] J.G. Gere, Mechanics of Materials, sixth ed., Brooks/Cole, Belmont, CA, 2004.

[9] Goodfellow Cambridge Ltd., Huntingdon, UK (supplier data).

[10] A.M. Karow, Biophysical and chemical considerations in cryopreservation, in: A.M. Karow, D.E. Pegg (Eds.), Organ Preservation for Transplantation, Dekker, New York, 1981, p. 113.

[11] C. Kroener, B.J. Luyet, Formation of cracks during the vitrification of glycerol solutions and disappearance of the cracks during rewarming, Biodynamica 10 (201) (1966) 47–52.

[12] B.J. Luyet, The vitrification of organic colloids and of protoplasm, Biodynamica 1 (29) (1937) 1–14.

[13] L.E. Malvern, Introduction to the Mechanics of a Continuous Medium, Prentice-Hall, Englewood Cliffs, New Jersey, 1969.

[14] P. Mehl, Nucleation and crystal growth in a vitrification solution tested for organ cryopreservation by vitrification, Cryobiology 30 (1993) 509–518.

[15] M.C. Palastro, P.S. Steif, Y. Rabin, Predictions of cracking during vitrification of cryoprotectants. CRYO 2005—The 42nd Annual Meeting of the Society for Cryobiology, Minneapolis, MN, July 24–27.

[16] D.E. Pegg, M.C. Wusteman, S. Boylan, Fractures in cryopreserved elastic arteries, Cryobiology 34 (2) (1997) 183–192.

[17] J. Plitz, Y. Rabin, J. Walsh, The effect of thermal expansion of ingredients on the cocktails VS55 and DP6, Cell Preservation Technology 2 (3) (2004) 215–226.

[18] Y. Rabin, M.J. Taylor, N. Wolmark, Thermal expansion measurements of frozen biological tissues at cryogenic temperatures, ASME Journal of Biomechanical Engineering 120 (2) (1998) 259–266.

[19] Y. Rabin, P.S. Steif, Thermal stress modeling of freezing biological tissues, in: Advances in Heat and Mass Transfer in Biotechnology, IMECE 1999, Nashville, Tennessee. ASME HTD-Vol. 363/BED-Vol. 44, 1999, pp. 183–188.

[20] Y. Rabin, P.S. Steif, Thermal stress modeling in cryosurgery, International Journal of Solids and Structures 37 (2000) 2363–2375.

[21] Y. Rabin, E. Bell, Thermal expansion measurements of cryoprotective agents. Part I: A new experimental apparatus, Cryobiology 46 (2003) 254–263.

[22] Y. Rabin, E. Bell, Thermal expansion measurements of cryoprotective agents. Part II: Measurements of DP6 and VS55, and comparison with DMSO, Cryobiology 46 (2003) 264–270.

[23] Y. Rabin, J. Plitz, Thermal expansion of blood vessels and muscle specimens permeated with DMSO, DP6, and VS55 in cryogenic temperatures, Annals of Biomedical Engineering 33 (9) (2005) 1213–1228.

[24] Y. Rabin, P.S. Steif, M.J. Taylor, J.R. Walsh, S. Baicu, Cryomacroscopy of vitrification: selected experiments on DP6 and VS55: <http://www.me.cmu.edu/faculty1/rabin/CryomacroscopyImages01.html/> (2005).

[25] Y. Rabin, P.S. Steif , K.C. Hess, J.L. Jimenez-Rios, Cryomacroscopy of fracture formation in vitrified thin films of cryoprotectants: <http://www.me.cmu.edu/faculty1/rabin/CryomacroscopyImages02.html/> (2005).

[26] Y. Rabin, M.J. Taylor, J.R. Walsh, S. Baicu, P.S. Steif, Cryomacroscopy of vitrification, Part I: A prototype and experimental observations on the cocktails VS55 and DP6, Cell Preservation Technology 3 (3) (2005) 169–183.

[27] Y. Rabin, P.S. Steif, Analysis of thermo-mechanical stress during cryopreservation of blood vessels, Cryoletters 26 (6) (2005) 409–411.

[28] D.W. Richerson, Modern ceramic engineering: properties, processing, and use in design, Marcel Dekker, Inc., New York, 1992.

[29] S.A. Schichman, R.L. Amey, Viscosity and local liquid structure in dimethyl sulfoxide-water mixtures, J. Phys. Chem. 75 (1) (1971) 98–102.

[30] Y.C. Song, B.S. Khirabadi, F.G. Lightfoot, K.G.M. Brockbank, M.J. Taylor, Vitreous cryopreservation maintains the function of vascular grafts, Nature Biotechnology 18 (2000) 296–299.

[31] P.S. Steif, M. Palastro, C.R. Wen, S. Baicu, M.J. Taylor, Y. Rabin, Cryomacroscopy of vitrification, Part II: Experimental observations and analysis of fracture formation in vitrified VS55 and DP6, Cell Preservation Technology 3 (3) (2005) 184–200.

[32] M.J. Taylor, Sub-zero preservation and the prospect of long-term storage of multicellular tissues and organs, in: R.Y. Calne (Ed.), Transplantation Immunology: Clinical and Experimental, Oxford University Press, Oxford, New York, Tokyo, 1984, pp. 360–390.
[33] M.J. Taylor, Physico-chemical principles of low temperature biology, in: B.W.W. Grout, J.G. Morris (Eds.), The Effects of Low Temperatures on Biological System, Edward Arnold, London, 1987, pp. 3–71.
[34] M.J. Taylor, Y.C. Song, K.G.M. Brockbank, Vitrification in tissue preservation: new developments, in: B.J. Fuller, N. Lane, E.E. Benson (Eds.), Life in the Frozen State, CRC Press, New York, 2004, pp. 603–641.